AD NUMBER

AD527922

NEW LIMITATION CHANGE

TO

Approved for public release, distribution unlimited

FROM

Distribution Controlled. All requests to Chief, Office of Naval Research, Dept of the Navy, Arlington, VA 22217

AUTHORITY

ONR ltr dtd 8 Oct 1998

AD NUMBER

AD-527 922

CLASSIFICATION CHANGES

TO **UNCLASSIFIED**

FROM **CONFIDENTIAL**

AUTHORITY

OCA; DEC 31, 1981

[redacted]

AD#527922

NORTHROP

Research and Technology Center

[redacted]

[redacted]

NRTC 73-38R

HIGH POWER CO LASER
SIXTH QUARTERLY AND SEMIANNUAL TECHNICAL REPORT (U)

November 1973

Prepared by

Northrop Research and Technology Center
W. B. Lacina, V. Dragoo, M. L. Bhaumik
G. L. McAllister, D. K. Rice, M. M. Mann

Contract N00014-72-C-0043

Sponsored by
ADVANCED RESEARCH PROJECTS AGENCY
ARPA ORDER NO. 1807

Monitored by
OFFICE OF NAVAL RESEARCH
CODE 421

NORTHROP CORPORATION
Northrop Research and Technology Center
Laser Technology Laboratories
3401 West Broadway
Hawthorne, California 90250

[redacted]

UNCLASSIFIED

SECURITY CLASSIFICATION OF THIS PAGE (When Data Entered)

REPORT DOCUMENTATION PAGE

READ INSTRUCTIONS BEFORE COMPLETING FORM

1. REPORT NUMBER: NRTC 73-38R	2. GOVT ACCESSION NO.
3. RECIPIENT'S CATALOG NUMBER	
4. TITLE (and Subtitle): High Power CO Laser, Sixth Quarterly and Semiannual Technical Report	5. TYPE OF REPORT & PERIOD COVERED: Sixth Quarterly and Semi-annual Technical Report
6. PERFORMING ORG. REPORT NUMBER	
7. AUTHOR(s): W. B. Lacina, V. Dragoo, M. L. Bhaumik, G. L. McAllister, M. M. Mann	8. CONTRACT OR GRANT NUMBER(s): N00014-72-0043
9. PERFORMING ORGANIZATION NAME AND ADDRESS: Northrop Research and Technology Center, 3401 West Broadway, Hawthorne, California 90250	10. PROGRAM ELEMENT, PROJECT, TASK AREA & WORK UNIT NUMBERS: ARPA Order No. 1806
11. CONTROLLING OFFICE NAME AND ADDRESS: Advanced Research Projects Agency, 1400 Wilson Blvd, Arlington, Virginia 22209	12. REPORT DATE: November 1973
	13. NUMBER OF PAGES: 51
14. MONITORING AGENCY NAME & ADDRESS (if different from Controlling Office): Office of Naval Research, Department of the Navy, Arlington, Virginia 22217	15. SECURITY CLASS. (of this report): [redacted]N
	15a. DECLASSIFICATION/DOWNGRADING SCHEDULE

16. DISTRIBUTION STATEMENT (of this Report)

None.

17. DISTRIBUTION STATEMENT (of the abstract entered in Block 20, if different from Report)

None.

18. SUPPLEMENTARY NOTES

None.

19. KEY WORDS (Continue on reverse side if necessary and identify by block number)

CO Laser,
Molecular Lasers
Electrical Discharge Lasers
High Power Lasers
Molecular Kinetics
Kinetics Generalizations
Unstable Resonators
Mode Theory
VV Rates
Gain Relaxation
Rotational Relaxation
High Efficiency
Energy/Power Measurements

20. ABSTRACT (Continue on reverse side if necessary and identify by block number)

(U) Effort on the High Power CO Laser program is reviewed. The program is directed toward the development of the required CO laser technology, the required component technology, and the design and construction of intermediate power laser devices. The results of analytical and experimental investigation of the basic characteristics of the laser and data from a high pressure electrically excited CO laser device are discussed.

DD FORM 1 JAN 73 1473 EDITION OF 1 NOV 65 IS OBSOLETE

UNCLASSIFIED

SECURITY CLASSIFICATION OF THIS PAGE (When Data Entered)

NRTC 73-38R

PROGRAM IDENTIFICATION (U)

ARPA Order No.:	1807
Program Code No.:	3E90
Name of Contractor:	Northrop Corporation
Effective Date of Contract:	1 August 1971 - 31 December 1973
Amount of Contract:	$3,065,967
[redacted]	N00014-72-C-0043
Program Manager:	Dr. M. M Mann (213) 675-4611, Ext. 2821
Program Scientist:	Dr. G. L. McAllister (213) 675-4611, Ext. 4975
Scientific Officer:	Director, Physics Program Physical Sciences Division Office of Naval Research Department of the Navy 800 North Quincy Arlington, Virginia 22217

Disclaimer: The views and conclusions contained in this document are those of the authors and should not be interpreted as necessarily representing the official policies, either expressed or implied, of the Advanced Research Projects Agency or the U. S. Government.

TABLE OF CONTENTS (U)

[redacted]

1.0 SUMMARY

(S) The long range objective of this program is to develop the necessary technology for a 1 - 2 MW average power, repetitively pulsed, diffraction-limited CO laser operating at an electrical efficiency of 50% or more. The work covered in this contract involves the design of intermediate power CO laser devices, the development of the required CO laser technology, and the construction of an intermediate power CO laser device.

(U) This program encompasses, on a best effort basis, the following major tasks:

(U) 1. The development of both steady state and transient kinetic models in order that realistic theoretical predictions of high energy device characteristics can be made.

(U) 2. Measurements of basic parameters of the CO laser at low pressures including: gain, saturation intensity, rates of vibrational cross-relaxation between CO molecules, transfer rates of CO and N_2, discharge characteristics, and spectral characteristics.

(U) 3. Measurements and characterization of a high pressure E-beam excited pulsed laser to experimentally determine transient operating parameters for high energy extraction.

(U) 4. The design and construction of a 500J/pulse diffraction-limited CO laser oscillator.

(U) 5. The development of line selection techniques for controlling the oscillator spectral output.

[redacted]

(U) Several scaling generalizations of the molecular kinetics calculations for a pulsed CO EDL were investigated and the results discussed in a technical report.[1] It was shown how all necessary parameters and quantities of interest can be scaled to analyze a specific problem in terms of more general classes of results. The sensitivity of the system response to various parameters, and the characterization of the gain saturation as a function of total radiation intensity were investigated. It was shown that the transient quantum efficiency is, to a good approximation, mainly dependent only upon the total energy deposition as a function of time. Some of the topics discussed in that report are summarized in Section 2.0 below.

(U) Experiments involving measurement of transient gain relaxation in a three-laser configuration described elsewhere[2, 3] have been continued. Techniques for obtaining data have been improved, and determination of partial pressures has been carried out more accurately. The main effort has been concentrated on verifying previous data and extending the results to different pairs of vibrational bands and different pressures. Initial investigations of rotational cross-relaxation effects have been carried out, but results at present are only qualitative and preliminary. It is hoped that the present experimental configuration can give data that will allow a more quantitative measure of the rotational rates, and if so, these will be reported in the future. It is also possible that some estimate or verification of (CO, N_2) VV rates may be accessible from this experiment.

(U) Experimental and theoretical studies of mode control and resonator design have been continued. A theory has been developed to explain how mode characteristics can be optimized for unstable resonators by means of varying mirror reflectivity, curvature, or aperture shape. This theory shows that modes can be made approximately geometric by

minimizing the diffractive contribution introduced by edge waves. A detailed discussion of this analytic investigation is presented in a technical report.[4] Experimental investigations were also carried out with a high gain 3.5 μm Xe laser with an unstable resonator to verify some of these predictions. A review of this work is given in Section 4.0.

(U) Detailed experimental investigations were carried out with the one liter device (Device No. 1) to determine effects of gas constituents and impurities on laser output characteristics. Careful calibration of instrumentation was performed to accurately and consistently measure laser output extraction and efficiency. As a result of this effort, demonstration of very high extraction and efficiency has been achieved. A specific output energy of 760 ±115 J/liter/atm at 63 ±14% efficiency has been attained experimentally. These are the highest values that have been attained in any laser system.

(U) The integration and assembly of the nominal 10-liter laser device (Device No. 2) has been completed and tests have begun. Initial tests indicate satisfactory operation of the system. In particular, the gas conditioning system has been operated successfully, through many cycles, yielding a near diffraction limited medium in the 10-liter laser plenum at pressures up to one atmosphere and near liquid nitrogen temperatures. The lasing tests have been limited so far, however, to outputs of approximately 150 J/pulse due to arcing along the sidewalls and optical windows. This low output is due to the low sustainer fields to prevent arcing and the small optical volume (~3 liters) which is restricted by the 3 inch optical windows used. Modifications are being implemented to remove this limitation, and lasing tests at over 500 J/pulse output energies are anticipated shortly. The review of the device construction, initial test results and problem areas are discussed in Section 6.0 of this report.

2.0 KINETIC CALCULATIONS AND GENERALIZATIONS - by W. B. Lacina

(U) Recently, several scaling generalizations of the molecular kinetics calculations for a pulsed CO EDL (containing CO and monatomic diluents only) were presented and discussed in a technical report.[1] It was shown how all necessary parameters and quantities of interest can be scaled to analyze a specific problem in terms of more general classes of results. The sensitivity of the laser response to various parameters, and the characterization of the gain saturation as a function of total radiation intensity were investigated. It was shown that the transient quantum efficiency is, to a good approximation, mainly dependent only upon the total energy deposition as a function of time. Some of the topics and results discussed in that report will be summarized briefly here.

(U) The physics of the present theoretical model for the analysis of the molecular kinetics of a pulsed CO EDL has been described in more detail previously.[1] Basically, the analysis consists of four systems of equations that couple the CO vibrational population densities, the (multiline) radiation intensities, the gas kinetic temperature, and the plasma kinetic parameters (electron density and temperature). Although the details will be omitted here, it is possible to make several reasonable approximations that allow certain general scaling laws to be formulated in terms of a small number of parameters. The most important of these are defined below:

$$x_v = n_v/N_{CO} \qquad \tilde{\gamma} = \gamma/\xi$$

$$\tau = p_{CO}t \qquad \tilde{W}_e = W_e/p_{CO}^2$$

$$f = 1 + (3/2)p_{tot}/p_{CO} \qquad \tilde{I} = I\xi/p_{CO}^2$$

$$\xi = \Delta\upsilon_{CO}/\Delta\upsilon_{tot} \qquad \tilde{E} = E/p_{CO}$$

where p_{CO}, p_{tot} are pressures, n_v and N_{CO} are vibrational and total number densities for CO, $\Delta\upsilon_{CO}$ and $\Delta\upsilon_{tot}$ are partial and total broadening linewidths, γ is the threshold loss coefficient, W_e and E are power and energy per unit volume, and I is intensity.

(U) The master equation expresses the transient evolution of the relative vibrational population densities x_v as a function of the scale time $\tau = p_{CO}t$. This is to be expected, since the electrical excitation is kept constant, and the dominant kinetic processes are (two-body) VV collisions. The master equation depends explicitly only upon the kinetic temperature and the scaled electrical excitation power density W_e/p_{CO}^2. Implicitly, however, it depends also upon the scaled threshold loss coefficient $\tilde{\gamma}$ for the cavity due to the oscillation condition, and upon the factor f due to kinetic heating. The set of parameters (T_{mol}, $\tilde{W}_e$, $\tilde{\gamma}$, f) is shown to completely characterize the problem, and all of the extensive additional input required in the computer code consists of fundamental physical constants. A variety of numerical results based on the complete computer analysis were presented and discussed to show the relative sensitivity of these parameters. One of the interesting conclusions was that, for a fixed temperature T_{mol}, the time t required to attain some specified value η/η_∞ for the optical extraction efficiency satisfies

$$p_{CO}t\tilde{W}_e^{5/6} = \text{const},$$

to a good approximation. This implies that (within a range of values of $\tilde{\gamma}$ which are suitably small) a "universal plot" of efficiency versus the parameter $\tilde{e} \equiv p_{CO}t\tilde{W}_e^{5/6}$ can be constructed, and examples of quantum power and energy efficiency as a function of $\tilde{e}$ are shown in

Figure 2.1 and 2.2. The significance of the parameter $\tilde{e}$ is obvious; if the exponent of $\tilde{W}_e$ were unity instead of 5/6, $\tilde{e}$ would represent the total electrical energy ($J/cm^3/torr$) which has been deposited up to time t. It was found that, in the range of temperatures from 60 - 300°K and for reasonably small values of $\tilde{\gamma}$, turn-on occurs (typically) after ~0.6 - 1.0 J/liter/torr has been deposited, and steady state is attained after ~1.9 - 2.6 J/liter/torr has been deposited.

(U) It is interesting to characterize the CO medium by a saturation intensity. Although the full kinetic model contains simultaneous oscillation on several lines, it is convenient to neglect this feature and observe how the gain saturates as a function of the total radiation intensity in the medium. For the analysis of a simple two-level model, it can be shown that the saturated gain $\alpha(I)$ satisfies

$$\alpha(I) = \alpha_o (1 + I/I_s)^{-1}$$

where the satuation intensity I_s is independent of the electrical pumping. It was shown that, in steady state, the CO EDL follows a simple dependence of this form, and an estimate of the scaled saturation intensity as a function of T_{mol} was obtained. Results of these calculations, which are described more fully in the report cited[1], are summarized in the table below.

(U) Table 2.1. Scaled Saturation Intensity. (U)

$T_{mol}(^oK)$	60	100	150	200	300
$\tilde{I}_s(W/cm^2/torr^2)$	0.6	0.8	1.6	2.5	6.4

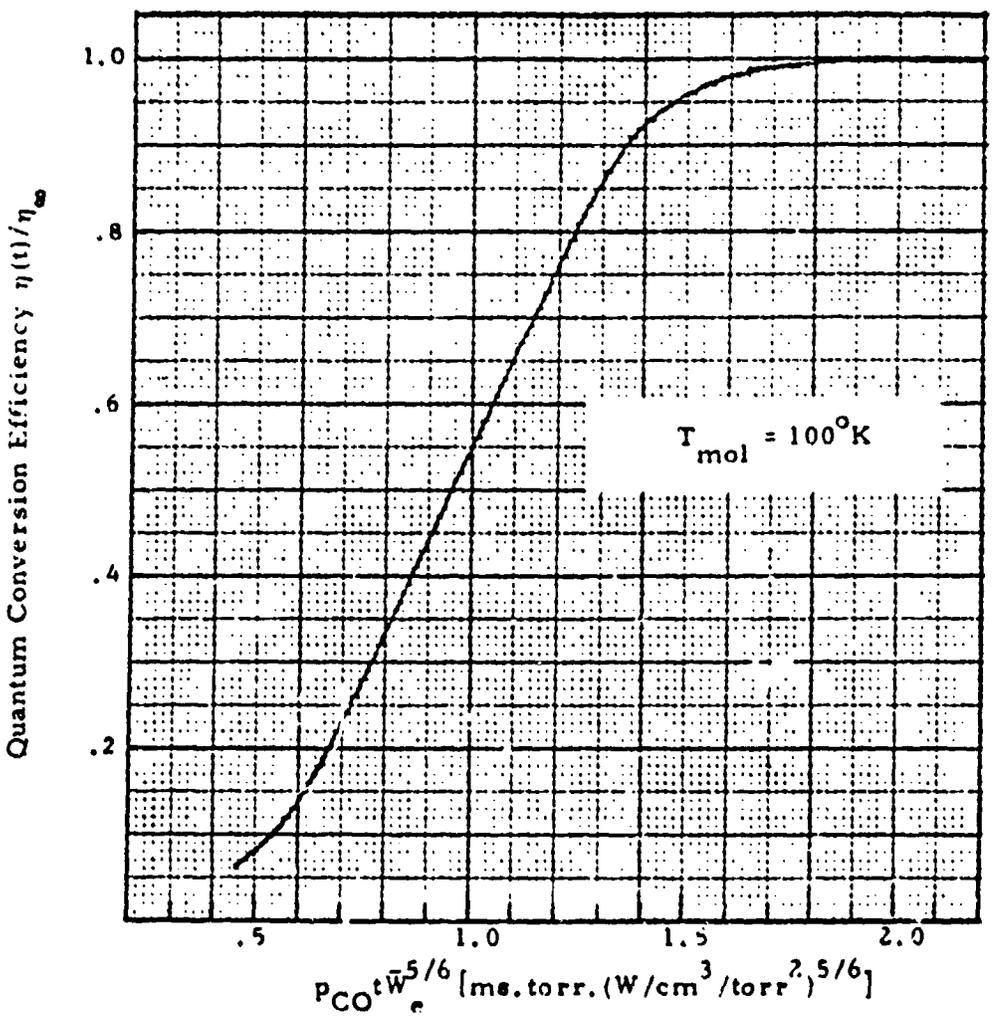

(U) Figure 2.1. Quantum power efficiency as a function of parameter $\tilde{e} = p_{CO}tW^{5/6}$. Note that $\tilde{e}$ is approximately energy deposited in units of J/liter/torr. (U)

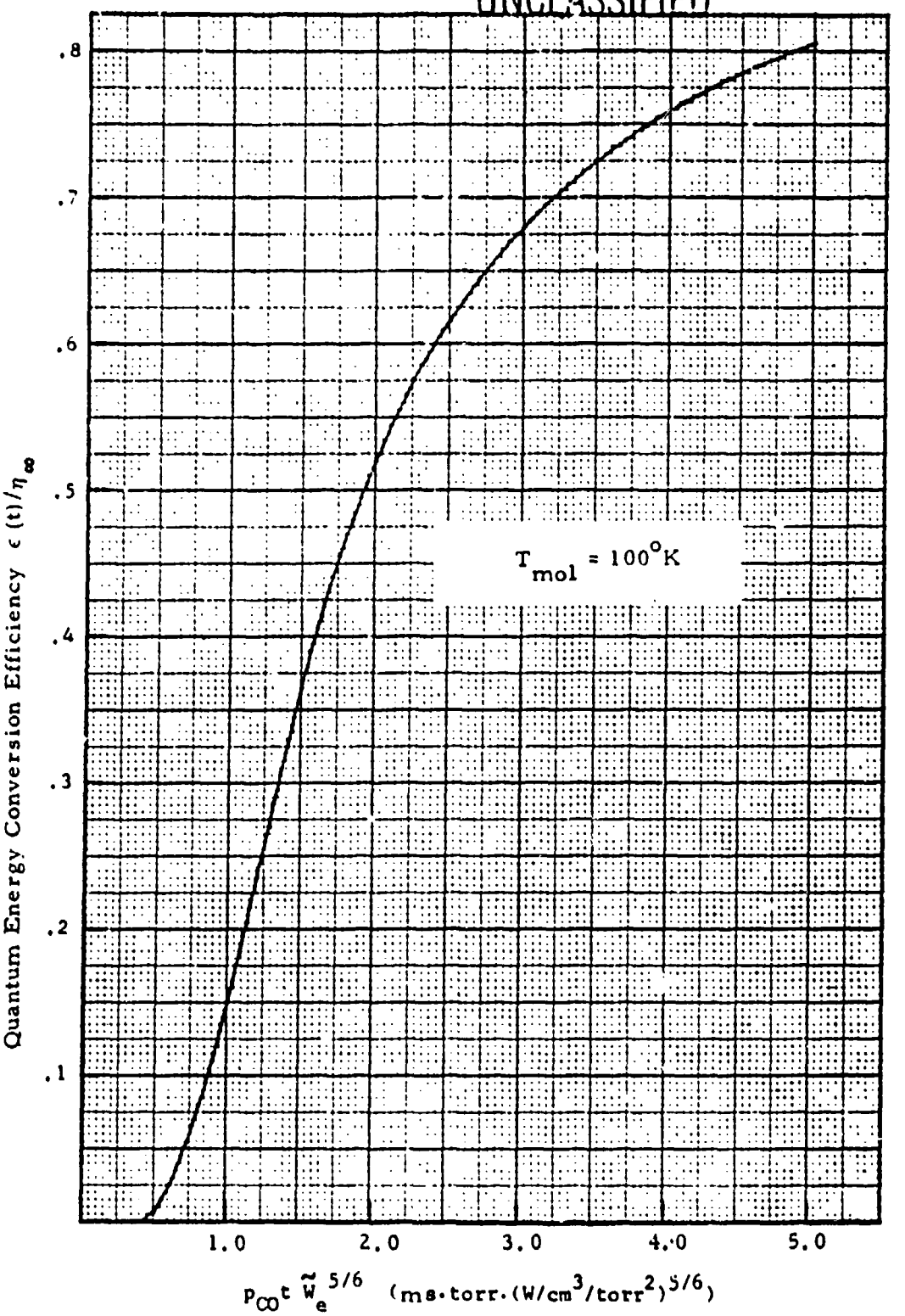

(U) Figure 2.2. Quantum energy efficiency as a function of parameter $\tilde{e} = p_{CO}tW^{5/6}$. Note that $\tilde{e}$ is approximately energy deposited in units of J/liter/torr. (U)

3.0 V-V RATE MEASUREMENTS - by V. Dragoo and M. Bhaumik

(U) A concerted effort has been made to obtain V-V rate measurements which agree with previously reported data[3] and to enlarge the data base to encompass more V level pairs. To date several experimental improvements have been made to enhance the reliability of the data.

(U) The most important of these improvements is the accurate determination of the laser gas constituents. Three techniques for gas partial pressure determination have been used: direct pressure readout from a "real pressure" vacuum guage, calibrated flow meter, and gas sampling using a mass spectrometer. Of these gas sampling is the most accurate. A sampling system is now in operation which provides partial pressure information to two significant figures. In addition the system allows assessment of the residual gas constituents present in the laser in the absence of gas flow. Also, the gas sampling system has verified the determination of partial pressure using the flow meter technique. The gas sampling system has to be regarded as the superior technique in that flow meter instabilities are common and that the gas sampling system has demonstrated a two significant figure accuracy.

(U) Figure 3.1 is a schematic representation of the sampling system. Needle valves 1 and 2 provide pressure drops between the laser supply line and the transfer line, and between the transfer line and the analyzing volume. The transfer line is pumped by the roughing pump to $\simeq 10\,\mu$. This provides for a fast response time. The sampled gas is analyzed with the UTI Mass Filter. Since nonlinearities in response of the mass filter do exist, particularly for inert gas species, calibration of the sampling system response is required. The calibration technique used here is to establish a flow of a single gas (CO, CO_2 or He) at a pressure

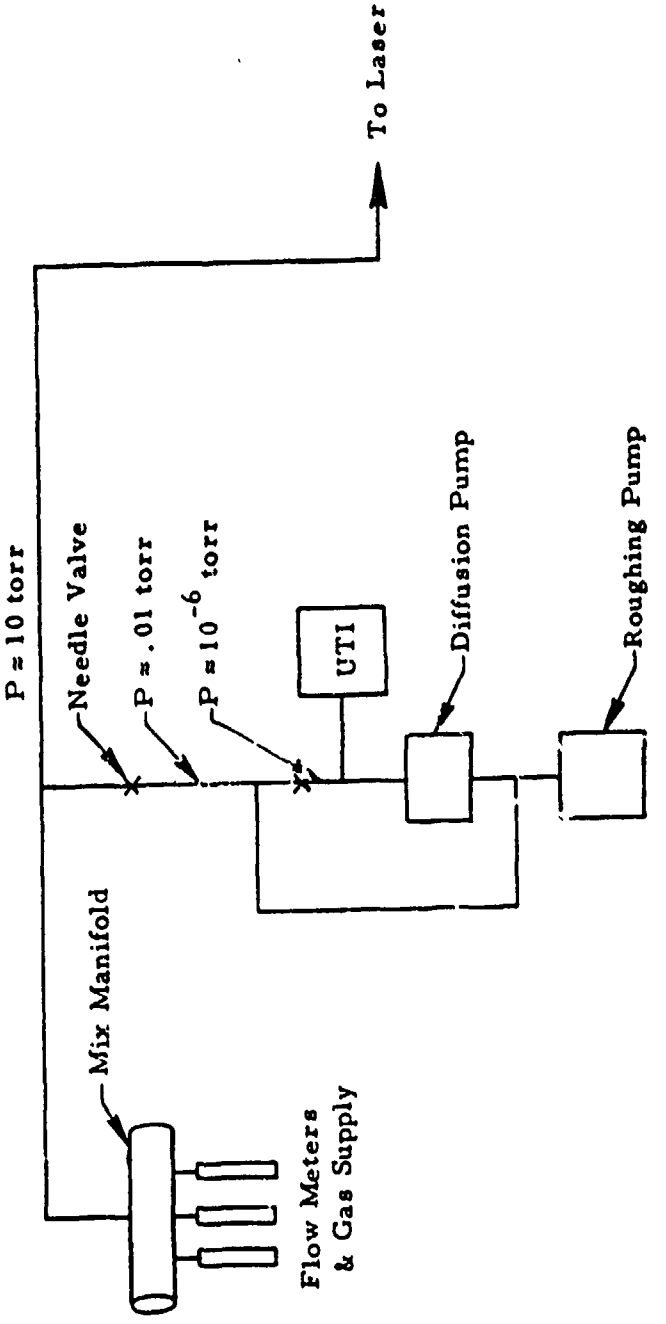

(U) Figure 3.1. Gas sampling system. (U)

of 5 to 10 torr in the laser tube. The mass selector of the UTI Mass Filter is set to the corresponding AMU and the response recorded. A similar pressure versus UTI response is measured for the remaining two gases. The calibration reveals that the sensitivity to CO and CO_2 are very nearly equal while the sensitivity to He is 0.36 that of CO.

(U) One of the more important results obtained from the gas sampling system is the effect of throttling the laser vacuum pump. Throttling the pump decreases the effective conductance of the laser vacuum system. Therefore, the pumping speed of the system versus pressure is no longer constant. This means that if CO only is allowed to flow, yielding a given pressure, subsequent addition of He at higher pressure will lower the resulting partial pressure of CO below its original value. This occurs simply because the vacuum system is more efficient at the higher pressure. This effect accounts for erroneous partial pressure data obtained from direct gauge readout. (The error is approximately 20% to 30%, depending on the total pressure.)

(U) Other improvements to the experimental apparatus included a lower pressure liquid nitrogen supply system, and acoustic isolation of key optical components. Previous LN_2 cooling apparatus operated with cooling jacket pressures as high as 10 to 12 psig. This elevated pressure raised the LN_2 temperature. The present system operates at 0.5 psig to insure a nearly atmospheric pressure LN_2 temperature.

(U) These modifications are now complete and V-V rate measurements are being studied using laser line pairs previously studied.[3] The line pairs under study are:

Saturation Laser	Probe Laser
8-7P(12)	9-8P(12)
8-7P(12)	9-8P(11)

(U) Figures 3.2 and 3.3 are representative traces of the relaxation signal for these laser line pairs. This data overlaps with previously reported results and extends the measurements to include higher CO partial pressures. At this point, the experiment is performing as expected and the short term goal is to extend the data base to include as many different laser line pairs as is possible. Emphasis will be on different vibrational pairs as opposed to different rotational levels between any given vibrational pair.

(U) In addition to the vibrational cross relaxation experiments, qualitative experiments designed to indicate rotational cross relaxation rates were performed. The experimental procedure was identical to the V-V rate measurements, except that the He partial pressure was adjusted over a wide range (5 to 20 torr), since the rotational relaxation mechanism depends on total pressure (as opposed to CO partial pressure in the case of V-V relaxation). In particular, a change in the transient gain characteristics of the laser medium should result for saturation laser (S) and probe laser (P) line pairs that do not involve rotational cascade processes. For example, laser line pairs of S:8-7P(12)/P:9-8P(11) and S:8-7P(14)/P:9-8P(11) differ in that the former pair shares a common rotational level. Figure 3.4 shows the energy level representation for the two cases.

(U) Figure 3.5 shows results of transient gain measurements for the 9-8P(11) line, corresponding to saturation laser lines of 8-7P(12)

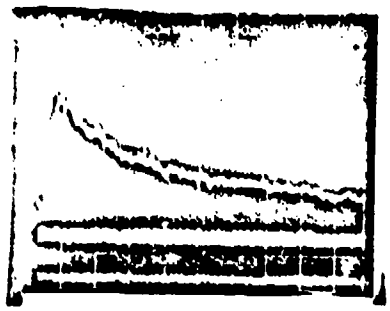

P_{CO}: 0.10 torr

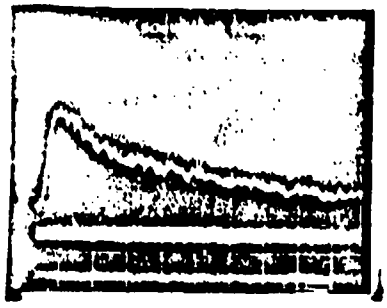

P_{CO}: 0.22 torr

P_{CO}: 0.45 torr

(U) Figure 3.2. Transient gain for 9-8 P(12) (probe) saturation laser at 8-7P(12). (U)

P_{CO} = 0.33 torr

P_{CO} = 0.52 torr

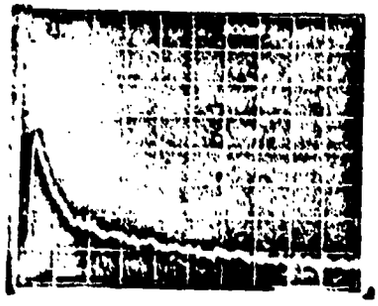

P_{CO} = 0.75 torr

(U) Figure 3.3. Transient gain for 9-8P(11) (probe) saturation laser at 807P(12). (U)

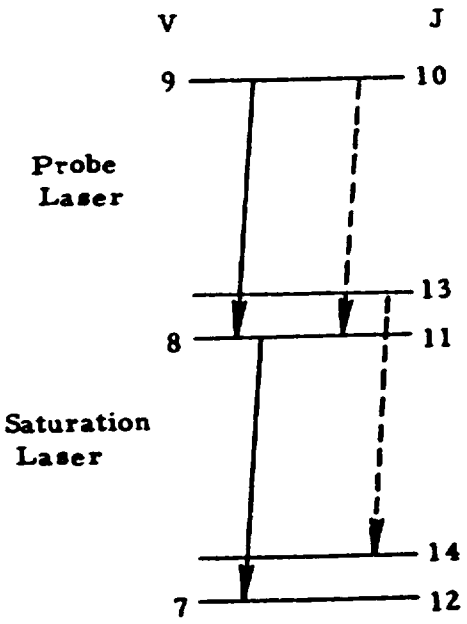

I: Saturation Laser 9-8P(11)
Probe Laser 8-7P(12) (Solid Arrows)

These levels share a common rotational/vibrational level

V = 8

J = 11

II: Saturation Laser 9-8P(11)
Probe Laser 8-7P(14) (Broken Arrows)

No common rotational level exists

(U) Figure 3.4. Energy level schematic for rotational cross relaxation measurements. (U)

P_T = 5 torr

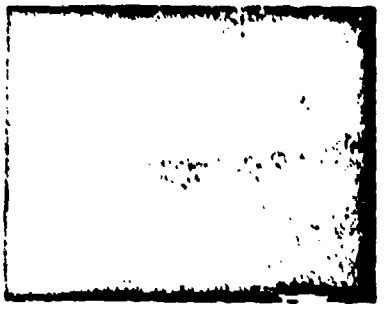

P_T = 5 torr

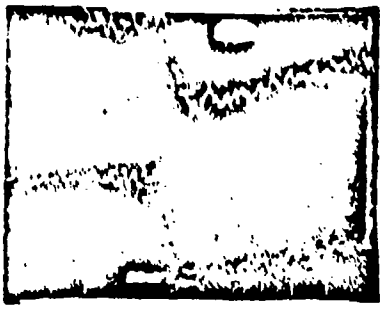

P_T = 10 torr

P_T = 19 torr

P_T = 20 torr

P:9-8P(11)

S:8-7P(12)

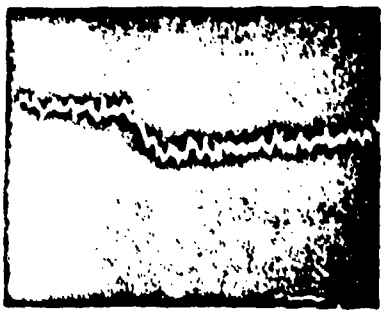

P_T = 20 torr

P = 9-8P(11)

S = 8-7P(14)

(U) Figure 3.5. Transient gain rotation cross relaxation. (U)

and 8-7P(14). The signal rise times for the S:8-7P(12)/P:9-8P(12) case are approximately equal at all pressures and are in all cases less than the S:8-7P(14)/P:9-8P(12) case. In addition, the signal rise times for the S:8-7P(14)/P:9-8P(12) decrease with increasing pressure indicating the rotational cross relaxation effect between levels J = 11 and J = 13.

(U) Since the rate of stimulated emission and rotational cross relaxation are comparable for the present saturation laser intensity, it is difficult to obtain a clear distinction of the rotational rate. At this point the data is considered only indicative of the effect and further experiments are needed to test the relaxation mechanism.

4.0 MODE CONTROL AND RESONATOR DESIGN STUDIES - by G. McAllister

(U) During this reporting period the investigation of mode improvement by altering the sharp edges of the resonator mirrors has continued. Previous numerical calculations of mode intensity and phase profiles have shown that the fundamental mode of an unstable resonator can be greatly improved by smoothing the sharp mirror edge either by tapering the reflectivity near the mirror edge or by rolling off the edge of the mirror to introduce a phase taper. The resulting modes have much flatter intensity profiles (reducing the peak mirror loading), have much smaller phase distortions (increasing the peak intensity on a target in the far field) and have improved discrimination ratios (making single-mode operation easier). A theory was developed which led to a criterion for optimizing these improvements. This criterion and related numerical calculations have been described in a previous report.[4]

(U) In addition to using amplitude and phase tapering to smooth the sharp edge of the mirror it should be possible to accomplish the same mode improvements by using a sharp edge mirror with a properly designed shape. Experimental results obtained using a 3.5μ xenon laser confirm that this is possible and indicate why unstable resonators have been quite successful in achieving good mode quality from high Fresnel number resonators. A brief description of the theory along with a description of the experimental configuration and experimental results follow.

4.1 Theory. (U) It has been pointed out by Ananev[5] that the diffracted wave from the sharp edge of an unstable resonator mirror (called an "edge wave") has a large effect on the resonator modes. In particular, that part of the edge wave directed such that it is reflected back into the cavity and is trapped along the axis will have a dominant effect on the mode. The

present work has been aimed at determining techniques for designing resonators which have fundamental modes that approach the fundamental geometrical optics mode, i.e., modes which have flat intensity profiles and spherical phase fronts. The criterion used for the resonator designs and the assumptions used in determining this criterion are summarized below for a symmetric, unstable resonator.

(U) One of the mirrors is first assumed to be uniformly illuminated with a spherical phase front as though the fundamental geometrical optics mode existed. The diffracted field at any point can be expressed, following Born and Wolfe[6], as the sum of a geometrical optics term plus a diffracted wave. The geometrical optics term is just an expanding spherical wave which appears as though it originated at the virtual focus[7] behind the mirror and the diffraction term, which is the edge wave contribution, can be expressed as a line integral around the mirror boundary. If the resonator can be designed such that the most significant edge wave contribution (that directed such that it becomes trapped along the resonator axis) can be minimized then the mode will become more like the geometrical optics mode which is desired. The phase shift between two trapped rays originating from different radii at the mirror is the same, after many round trips, as the phase difference between the two rays if they are extended directly to the virtual focus beyond the opposite mirror. Thus the diffraction contribution to the mode can be minimized by designing the resonator so that the edge diffracted field amplitude at the opposite virtual focus is a minimum.

(U) The diffracted field amplitude at that point is given by

$$U_D(P) = \frac{-U_o \exp(ikR)}{R} \int_1^{\rho_M} \exp(i2\pi N_{eq}\rho^2)\rho\, d\rho \quad (1)$$

where ρ is the normalized radius at the mirror, r/a, ρ_M is the maximum mirror radius, R is the distance between the virtual foci and

N_{eq} is the equivalent Fresnel number computed at r = a. An optimum mirror shape can be calculated which will result in Eq. (1) going to zero and is described by the transcendental equation

$$\cos\left(2\theta - \sqrt{\rho^4 - 1}\right) = 1/\rho^2. \qquad (2)$$

However, the primary consideration is that the boundary must cover an even number of equivalent Fresnel zones. That is, we require that

$$N_{eq}(\rho = 1) = N_{eq}(\rho = \rho_M) - m \qquad (3)$$

where m is an integer. When this condition is fulfilled for a typical mirror shape the phases of the edge wave contributions will interfere destructively and result in a small field amplitude as calculated by Eq. (1). We have looked at the fundamental modes for mirrors with several shapes and have found, as described below, that when the boundary is distributed over two equivalent Fresnel zones the mode is indeed improved over that for a circular mirror.

4.2 Experimental Configuration. (U) A 3.5μ longitudinal discharge He-Xe laser was constructed to study the modes because the high gain allows the use of large magnification resonator configurations with reasonably short gain lengths. The intensity and stability of the modes varies somewhat with the discharge pressure, gas mixture ratios and discharge current, but the mode shapes are largely independent of these parameters. Typical operating parameters are P_{He} = 200 μ, P_{Xe} = 10μ with a discharge current of 75 mA. The discharge is 1 cm in diameter, 25 cm long and the tube is sealed at the ends with AR coated CaF_2 windows.

(U) One of the mirrors forming the unstable resonator consists of an AR coated CaF_2 lens with a silver spot of the desired shape deposited on it. The second mirror consists of a similar CaF_2 lens with a 90% reflectivity dielectric coating deposited on it. The 10% transmission through this coating is used to couple out a signal to observe the mode pattern. This output is directed by a rotating flat onto another flat mirror used to align the external beam such that it sweeps by the detector element of a Ge:Au detector. Thus an intensity profile is displayed in time on an oscilloscope trace.

(U) Mirror alignment and bore sighting both have a large effect on the mode profiles and must be done carefully. Initial alignment is achieved using an external He-Ne laser and final alignment is made electronically with a piezoelectric orientation mount used as the mount for the back mirror. Misalignment angles of less than 50μ rad are sufficient to introduce severe assymetries in the mode profiles.

4.3 Experimental Results. (U) The analytical investigation described above indicates that noncircular mirror shapes may produce considerable improvements in the resonator mode. We have studied the mode intensity profiles for several mirror designs and have found that they can be improved by proper design. Comparisons for the three mirror shapes shown in Figure 4.1 are shown in Figure 4.2.

(U) The circular mirror illustrated in Figure 4.1A is 5 mm in diameter and results in an equivalent Fresnel number of 2.5 for the resonator used. The corresponding mode shape is shown in Figure 4.2A and shows the intense spikes characteristic of circular mirrors with sharp edges.

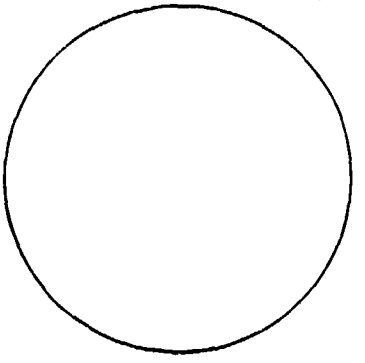

A. Circular Mirror. $N_{eq} = 2.5$.

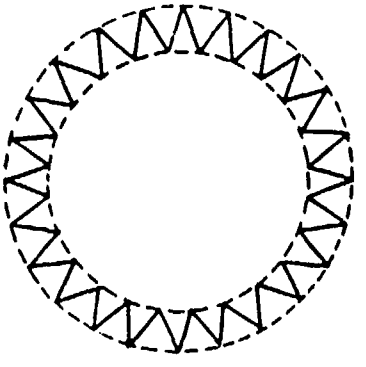

B. Serrated Mirror. $N_{eq_{MAX}} = 2.5$, $N_{eq_{MIN}} = 1.5$.

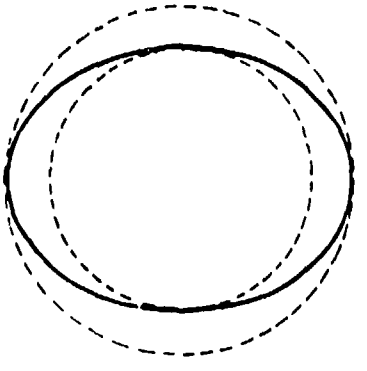

C. Elliptical Mirror. $N_{eq_{MAX}} = 2.5$, $N_{eq_{MIN}} = 1.5$.

(U) Figure 4.1. Mirror shapes used for comparison of mode intensity profiles. (U)

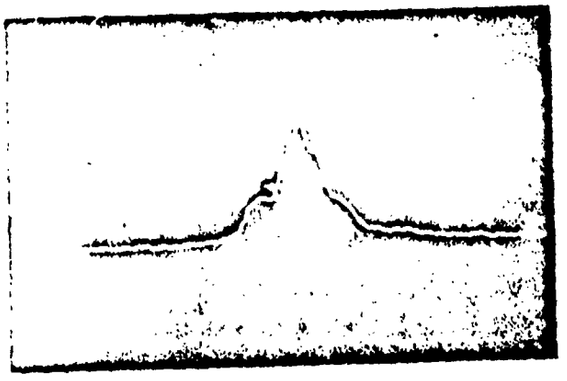

A. Circular Mirror Intensity Profile

B. Serrated Mirror Intensity Profile

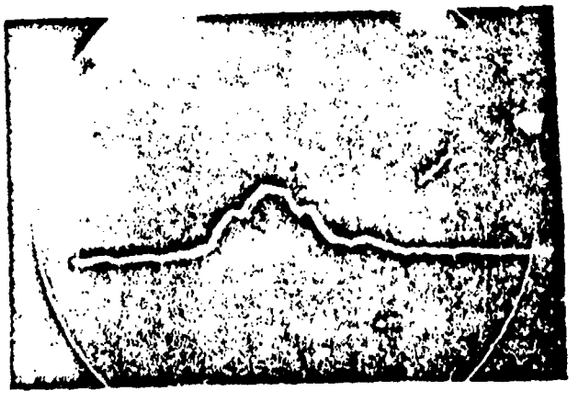

C. Elliptical Mirror Intensity Profile

(U) Figure 4.2. Intensity profiles for the mirror shapes illustrated in Figure 4.1. (U)

(U) The serated mirror illustrated in Figure 4.1b has a boundary that varies rapidly between a maximum diameter of 5 mm which results in $N_{eq} = 2.5$ and a minimum diameter of 3.9 mm which results in $N_{eq} = 1.5$. Although the serated edge does not follow the optimum curve described by Eq. (2) it does cover two equivalent Fresnel zones and improvement is expected. The corresponding mode intensity profile given in Figure 4.2b shows that the intense diffraction spikes characteristic of the circular mirror are gone and that the intensity profile is much more nearly uniform.

(U) Similar improvements are seen in Figure 4.2c corresponding to the elliptical mirror of Figure 4.1c. Again the mirror covers two equivalent Fresnel zones and in this case the boundary follows very nearly along an optimum boundary described by Eq. (2).

(U) Improvements of this kind are readily achievable because of the ease with which the mirror boundary can be shaped. It should be a pointed out that resonators which are typically used often automatically incorporate these improvements. Many high volume, high energy lasers employ square or rectangular discharge areas and thus use square or rectangular mirrors. The mirror boundaries automatically cross several equivalent Fresnel zones and even if they are not optimally designed will be a significant improvement over circular mirrors. In addition, for very large Fresnel number resonators the outer two equivalent Fresnel zones occupy a very small fraction of the radius and imperfections in the mirror shape and surface will again lead to mode improvements.

5.0 EXPERIMENTAL INVESTIGATIONS WITH THE NOMINAL ONE LITER DEVICE - by D. K. Rice

(U) During this reporting period detailed experimental investigations with the one liter device were performed to accomplish three major objectives: (1) to determine the effects of gas constituents (including impurities) on the output characteristics of the laser, (2) to improve the reliability and consistency of operation of the laser, and (3) to carefully identify the calibration and the error bounds of the instrumentation for a consistent and accurate determination of the energy extraction efficiency of the laser. As a result of these efforts, experimental demonstration of the extremely high CO laser efficiencies predicted by theoretical calculations have been achieved. Table 5.1 summarizes a comparison between experimentally obtained data and predicted values of efficiency and extraction for a CO EDL. The tabulated experimental efficiency is the ratio of optically extracted energy to electrical input energy into the entire discharge volume. The actual radiative conversion efficiency is higher since the optical volume is only 75% of the discharge volume. However, due to the nonuniformity of the excitation as discussed in Section 5.3, the magnitude of this factor cannot be accurately estimated. The maximum measured efficiency was obtained in a CO/Ar mix of 1/10, while the maximum energy was obtained in a CO/N_2 mix in the same ratio. The specific energy and efficiency that have been experimentally demonstrated for the CO EDL are the highest ever achieved by any laser.

(U) Table 5.1. Comparison of Measured and Predicted CO EDL Characteristics. (U)

	Measured	Predicted
Efficiency	63 $\pm$14%	85%
Specific Energy	760 $\pm$115J/ℓ -atm	1.0 KJ/ℓ - atm
	180 $\pm$40 kJ/kg	250 kJ/kg

5.1 Performance Improvement. (U) In previous experimental runs with the one liter laser system each run was limited to 10 to 20 shots due to the clouding of the cold laser IR windows after a one hour run. Since the definitive effect of the clouding was unknown, the extraction of significant parametric data after the start of clouding was questionable. The clouding eventually increased to the point where laser action was precluded. It was discovered that two factors were the cause of clouding: (1) formation of frost on the external surface of the windows, (2) formation of an unknown contaminant on the internal surfaces of the windows. The second problem was not noticed until the first was eliminated.

(U) Previously, the region between the cold window and the resonator mirror on each end of the laser was maintained with a mechanical pump at a pressure of several torr. This pressure was assumed to be sufficient to prevent water vapor from condensing onto the laser windows. This assumption was found to be in error from the following simple calculation. The rate of frosting can be approximated by determining the flux of water molecules incident upon the cold window, assumping that each impinging molecule is absorbed. The flux of molecules/cm^2/sec at 300°K, may be approximated by

$$\phi = n_{H_2O} v_x = n_{H_2O} \sqrt{2/3 \ kT/m_{H_2O}} = n_{H_2O} \times 1.3 \times 10^5$$

where, n_{H_2O} = number density of water molecules/cm^3 and v_x = the normal component of the thermal energy in cm/sec.

) For typical atmospheric conditions, the partial pressure of water vapor is approximately 10 torr, leading to $n_{H_2O} \cong 3.5 \times 10^{17}/cm^3$. For these conditions, the flux per μm. of total pressure is

$$\phi \cong 6 \times 10^{17} \text{ molecules/cm}^2\text{/sec/ } \mu\text{m.}$$

(U) The performance of the device will certainly be unacceptably degraded if the optical thickness of the adsorbed layer is equal to that of a 100 meter atmospheric path (corresponding to 3.5×10^{21} molecules/cm^2). Thus the allowable run time is approximately

$$T \simeq \frac{1000}{(\text{pressure in } \mu m)} \text{ minutes.}$$

(U) Obviously the analysis presented here can easily be off by an order of magnitude. However, it is evident that the required pressures are in the μm range. This requirement was met by inserting a large liquid nitrogen cold trap between the mechanical pump and window/mirror region on each end of the laser. The pressure in this region should be maintained at approximately 10 μm. This was successfully accomplished and thus, the frosting problem has been completely eliminated.

(U) It was discovered following solution of the frosting problem, that a second window contamination problem existed. Within 3/4 hour to one hour subsequent to achieving the typical cryogenic operating condition of the device, a brown tinted pattern started to form on the internal side of the windows.

(U) A very thorough investigation was undertaken to determine the source of the deposition pattern formation. The patterns were of an elliptical shape which suggested possible gas flow dependence. However, changing gas flow rates or plenum pressures had no direct effect on the shape or intensity of the pattern. The gas mixture used during the cool-down procedure was found to have no effect; the pattern began forming at approximately the same time during the cool-down whether nitrogen or argon was used.

A UTI Model 100C Precision Mass Analyzer was connected to the cold gas inlet to the laser plenum and to the exhaust part of the plenum. There was no significant difference detected in either the major or minor gas constituents between the inlet and exhaust with this instrument. Although it had been assumed that any contaminants in the gas supply would be trapped in the liquid nitrogen heat exchanger prior to reaching the laser plenum, a sample of the gas was sent for chemical analysis. Again nothing significant appeared.

(U) The gas samples were then taken directly from the laser plenum at various times during a cool-down and warm-up cycle using only the nitrogen supply. These samples were chemically analyzed. It appeared as if there were an excessive amount of oxygen in the system at cryogenic temperatures. This result seemed to indicate leaks of ambient air into the laser plenum. An extensive effort was thus made to seal the system using the UTI Precision Mass Analyzer as a leak detector. This effort was found to have no effect on the window contamination problem. However, the sealing of these leaks was subsequently found to have a significant effect on the laser performance. This is not surprising in retrospect since the presence of the smallest amount of atmospheric gas constituents has previously been observed to have profound effect on the operation of low pressure longitudinal discharge lasers.[8-12]

(U) Since the supply gas and ambient air were eliminated as sources of the window problem, it appeared that the contamination originated inside the laser plenum. All of the various materials used inside the chamber were tested under vacuum using the UTI instrument to identify any outgassing components which could possibly contribute to the contamination. No evidence was found to indicate this possibility.

(U) The calcium fluoride windows themselves or the thin film anti-reflection coatings were also examined as possible contributors to the problem. This was shown not to be the case when a cool-down/warm-up cycle was made using polycarbonate windows in place of the actual laser windows and the brownish tinted pattern appeared as usual.

(U) Cycle dependent characteristics of the deposition were also determined. Once the pattern formed, it could not be removed by changing the gas composition, gas flow rate, or plenum pressure; it could only be removed by allowing the system to warm-up. The pattern changed shape and location on the windows as the plenum temperature approached ambient. The pattern disappeared at approximately the same time during every warm-up cycle. There was no trace of contamination on the window surfaces when the system was disassembled following a cool-down/warm-up cycle. Frequently at a similar time in the warm-up phase, it would appear as if the pattern extended throughout the region between the windows as a stratified brownish colored gas; this situation would last for approximately five minutes. Occasionally during the warm-up phase dark particles would appear suspended in this region and then disappear.

(U) The problem still has not been identified but has been eliminated. As a result of using extremely high gas flow rates during the cool-down phase and thus reaching cryogenic temperature operating conditions very quickly, the formation of the window pattern was eliminated for the duration of any laser experiments. The pattern still forms during the warm-up phase only and does not interfere with the experiments. It is conjectured that the minute traces of contaminants, if they exist, are trapped in the heat exchangers under the normal operating conditions of the laser.

(U) After solving the problems of laser cold window frosting, the elimination of the brown tinted pattern formation on these windows, and minimization of leaks from the ambient atmosphere into the laser plenum chamber, reliable and consistent operation of the laser was achieved. This is illustrated by an experimental run consisting of 150 pulses with an average of 3 to 5 minutes between pulses.

5.2 Instrument Calibration for Energy Extraction Measurements. (U) In order to improve the accuracy of the parametric investigation of energy extraction from the nominal one liter CO EDL, a thorough and extensive effort was made to identify the calibration and the error bounds of the instrumentation used to measure the input and output energies of the laser.

(U) The experimental configuration for diagnostic studies of the laser are illustrated in Figure 5.1. The energy output is measured using the calcium fluoride beam splitter, the collecting/focusing mirror, and the calorimetric thermopile. The beam splitter has an antireflection coating on one surface; the reflectance of this component was measured to be 0.027 ± 0.001. The collecting/focusing mirror has a reflectance of 0.98 ± 0.005. The energy detector is an F&H Manufacturing Company Model E21 Calorimetric Thermopile. A careful series of measurements were made to establish a reliable calibration factor for this device. The unit was illuminated with broadband low level energy from a blackbody source, cw CO laser radiation from a longitudinal discharge laser, and radiation from a pulsed ruby laser. The device was also compared to several other laser power/energy meters. The calibration factor for the unit was determined to be 19μ V/J $\pm 5\%$ for a peak readout. The calorimeter output is recorded using a Keithley Model 160 Multimeter and a Hewlett Packard Model 7101B strip chart recorder. Considering all of the components and errors introduced in reading of the recorder trace, the rms error in the measurement of the output energy of the laser was determined to be $\pm 7\%$.

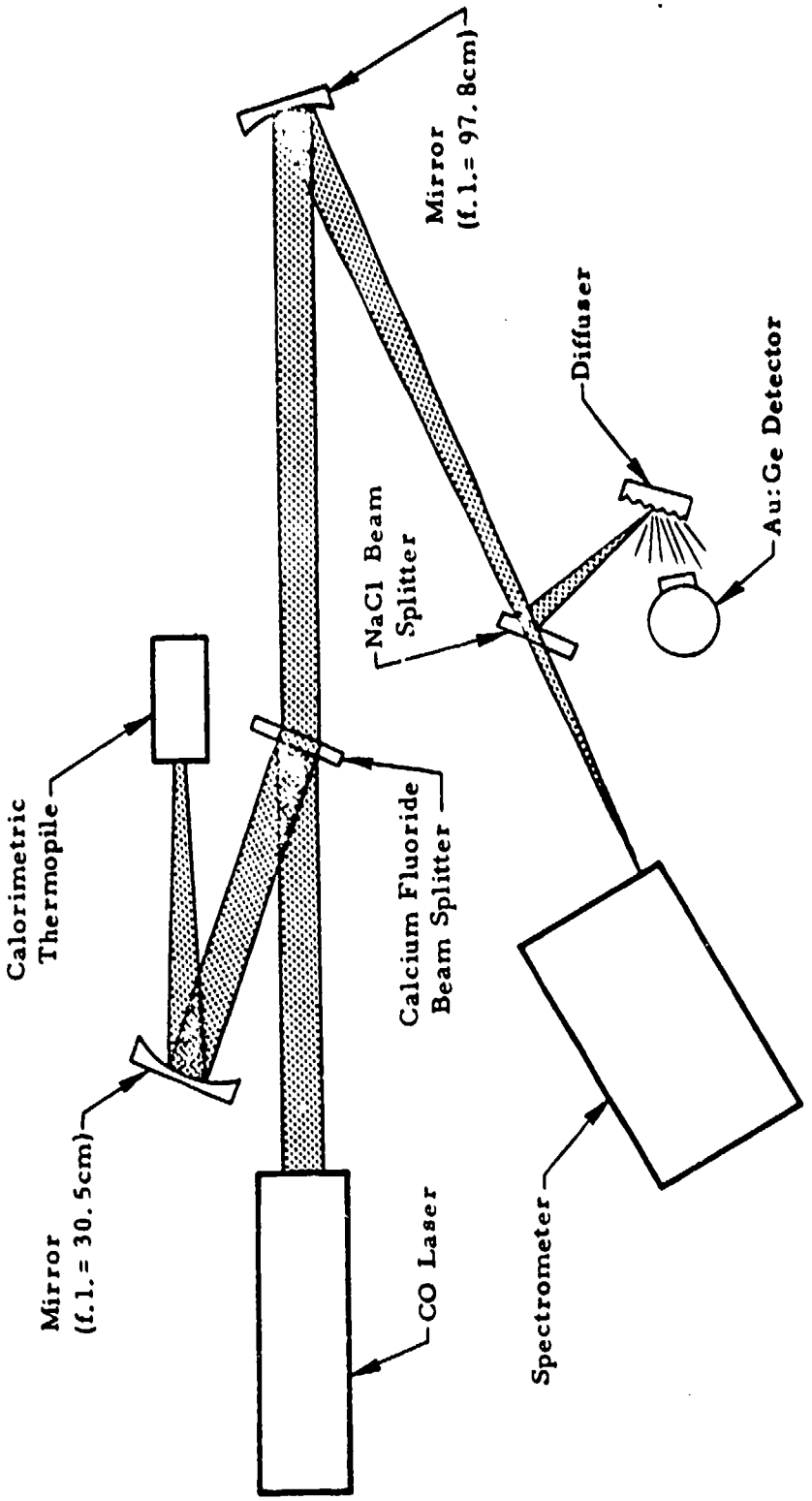

(U) Figure 5.1. Diagnostic Setup for CO EDL Device No. 1. (U)

(U) The electrical schematic of the measurement system used to determine the input energy is shown in Figure 5.2. The current probe is a Pearson Electronics Model 301X and has a measured accuracy in the pulsed mode of ±1%. The high voltage probe is a Tektronix Model P-6015, whose accuracy for the measurements is ±10%.* A Tektronix Model 549 Storage Oscilloscope with a Type 1A4 amplifier plug-in was used; the accuracy of the voltage calibration source is ±3% and the gain of the amplifier plug-in is ±3%. The voltage and current were read at various temporal points in the pulse from a recorded photograph and integrated numerically to determine the total energy input. Considering the possible errors in the measurements as well as that in reading the voltage/current photograph, the rms error in the measurement of the input energy to the laser is ±15%. Combining the cummulative errors of the input and output measuring instruments and components, it was determined that the overall laser efficiency measurement has an error bound of ±22%.

5.3 Experimental Results. (U) The increase in operation time and the elimination of contamination effects as discussed in Section 5.1 permitted a more extensive investigation of the nominal one liter CO EDL performance as a function of gas composition, and led to high efficiencies discussed in the beginning of this section. The nominal parameters of the laser are listed in Table 5.2.

*When the voltage probe is calibrated to the oscilloscope the accuracy error can be reduced to that of the oscilloscope and amplifier plug-in. (U)

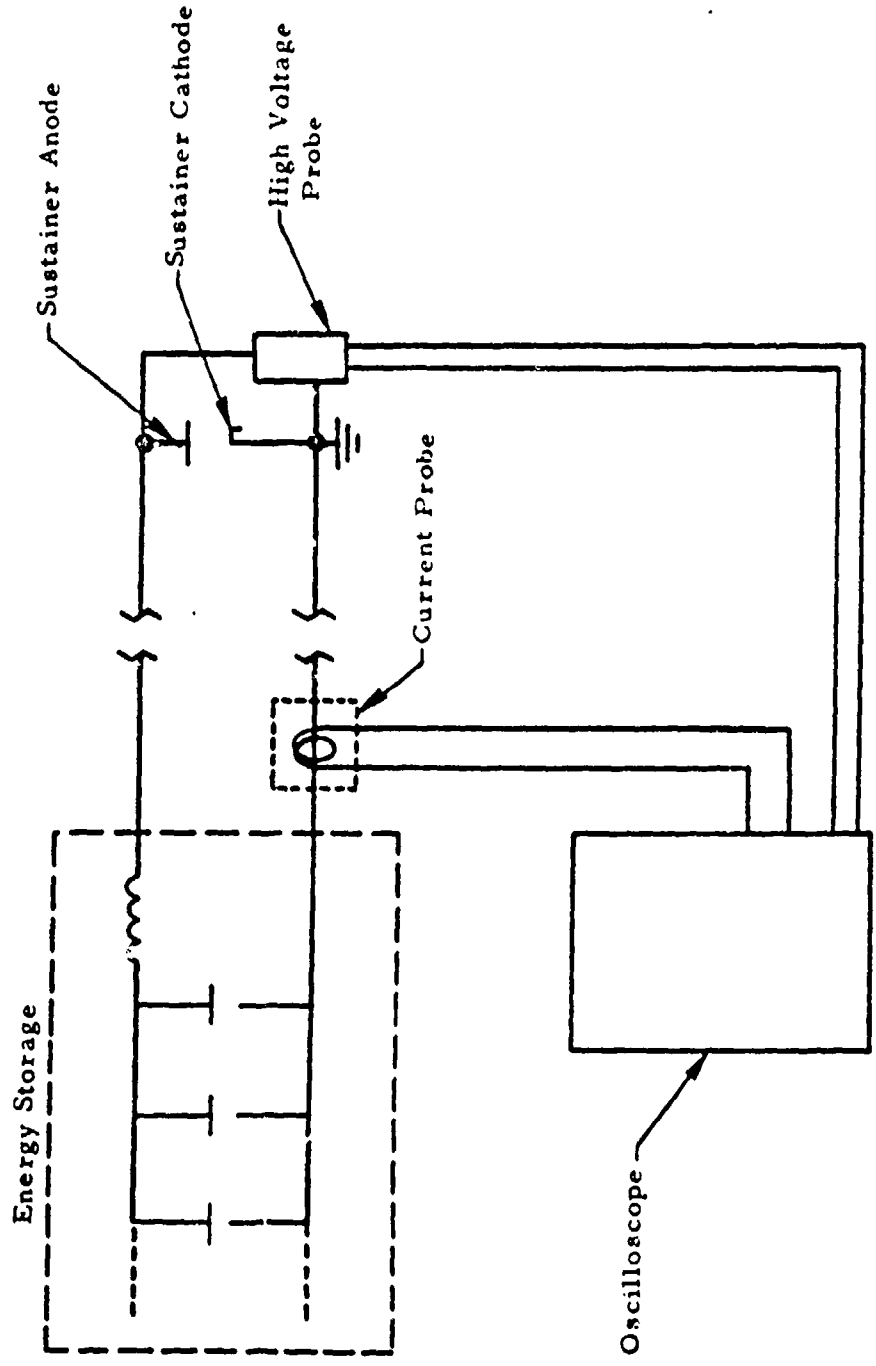

(U) Figure 5.2. Input Energy Measurement Schematic for CO EDL Device No. 1 (U)

(U) Table 5.2. Nominal CO Electric Discharge Laser (No. 1 Device) Parameters. (U)

Discharge Volume	2 Liters (4 x 5 x 100 cm)
Optical Volume	1.5 Liters
Gas Constituents	CO, N_2, Ar
Temperature	100°K
Pressure	100 torr
E-Beam Current Density	20 mA/cm^2
Sustainer Field	1 KV/cm
Sustainer Current Density	2 A/cm^2
Excitation Pulse Duration	100 μs

(U) The laser performance with CO/N_2 and CO/Ar gas mixtures was evaluated. Typical input/output characteristics for these cases are illustrated in Figure 5.3. In this figure the top oscilloscope trace is the laser output as monitored with the Au:Ge detector (see Figure 5.1). The center trace is the sustainer voltage (5 kV/div) and the bottom trace is the sustainer current (500A/div). Note that the energy extraction is higher with a CO/N_2 mixture than from a CO/Ar mixture. However, the extraction efficiency is higher with argon as the diluent gas. The reason that higher energy extraction is higher with nitrogen as the additive gas can be observed by comparing the temporal shapes of the output pulses in Figures 5.3a and 5.3b. The energy in the portion of the pulse following termination of the electrical excitation in the CO/N_2 case is comparable to that during excitation, while in the CO/Ar case it is much lower. During the electrical pulse both the CO and N_2 molecules are directly excited; the transfer of energy from the nitrogen molecules by vibrational exchange collisions continues after the direct electrical excitation has terminated. Thus a significant amount of energy has been stored in the vibrational bands of nitrogen and is available for extraction following the excitation pulse.

(U) The effect of energy storage in the nitrogen vibrational bands is further demonstrated by the results shown in Figure 5.4. The identification of the traces is the same as in Figure 5.3. The scales for the sustainer voltage and current are 2 kV/div and 200 A/div respectively. Figure 5.4a demonstrates the situation for essentially an equal concentration of nitrogen and carbon monoxide. In this case the direct electrical excitation of the carbon monoxide molecules is the dominant mechanism and thus most of the output energy occurs simultaneously with the excitation pulse. Figure 5.4b illustrates the results for a concentration of one part

T = 100°K

P = 100 torr

I_{gun} = 20 ma/cm^2

DISCHARGE VOL = 2.0 Liters

OPTICAL = 1.5 Liters

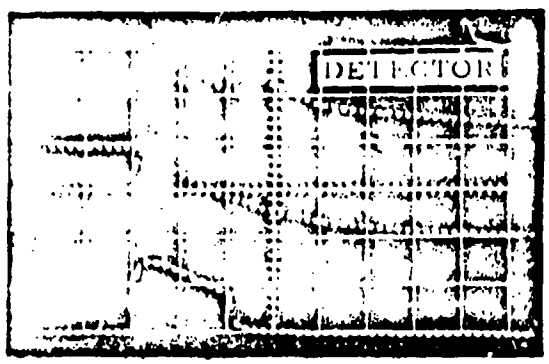

(a)

CO/N_2 = 1/10

U_o = 200 ± 25J

η_{TOT} = 48 ± 11%

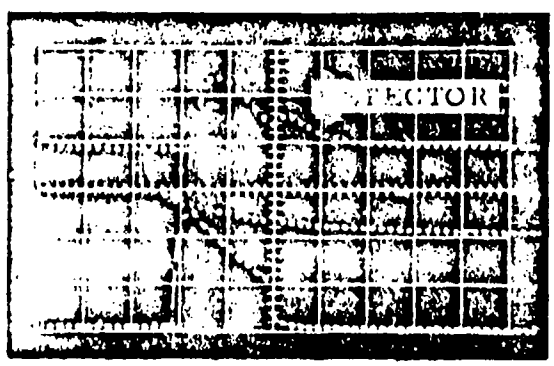

(b)

CO/Ar = 1/10

U_o = 153 ± 15J

η_{TOT} = 63 ± 14%

Time = 50 μs/Div

(U) Figure 5.3. Input/Output Characteristics of CO EDL (Device No. 1). (U)

(U) Figure 5.4. Output of CO EDL (Device No. 1). (U)

CO to 1000 of N_2 where a very small portion of the output occurs during the excitation period. In Figure 5.4c the extreme case is shown where essentially all of the energy is contained in the after pulse. In this situation there is relatively little direct excitation of the CO molecules; all of the electrical input is stored in the nitrogen vibrational bands and is transferred by collisional processes to the carbon monoxide molecules.

(U) Typical output spectra for the nominal one liter CO EDL is shown in Figure 5.5. This spectra is obtained from a photograph of the fluorescent screen of the Optical Engineering Spectrum Analyzer in the configuration of Figure 5.1. The spectra corresponds to the input/output data given in Figure 5.3. Note that there is no significant difference between the spectral outputs for these two cases. The energy in both situations is concentrated in the vibrational bands 7-6 and below. As discussed in previous reports, the current aspect ratio of the laser discharge region precludes sufficient electrical pumping to limit laser oscillation to the vibrational bands 6-5 and below; these are the bands which contain the rotational lines predicted to have high atmospheric transmittance.

(U) Modifications are being made to the nominal one liter plenum to alter the height-to-width aspect ratio of the discharge. This modification will permit a more uniform excitation of the discharge

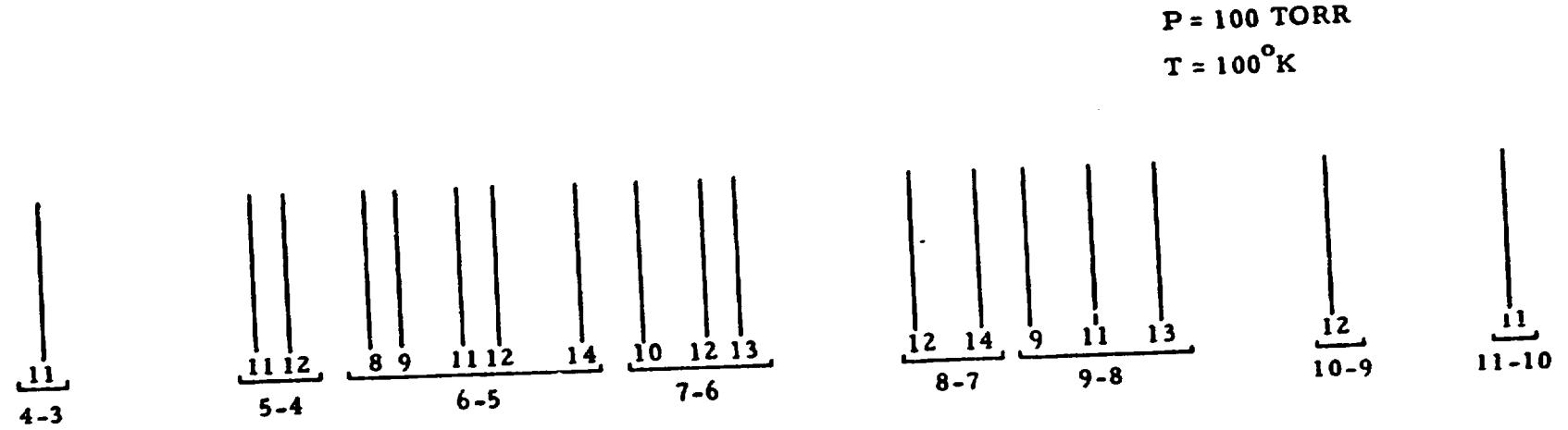

$CO/Ar = 1/10$; $P_{IN} = 2.2 - 0.4$ kW/cm^3

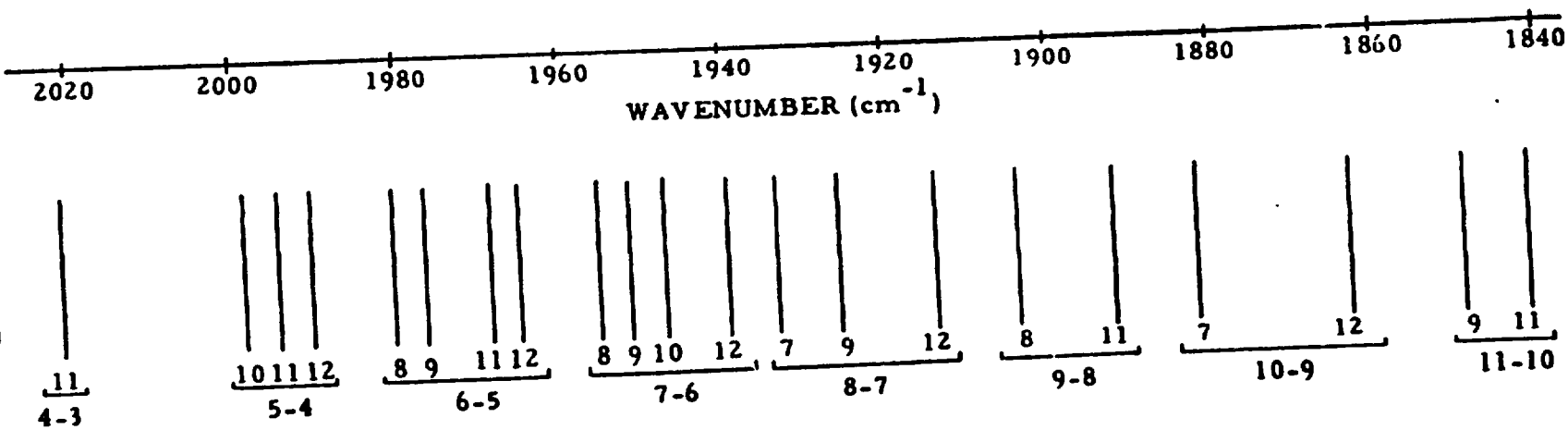

$CO/N_2 = 1/10$; $P_{IN} = 3.2 - 1.0$ kW/cm^3

(U) Figure 5.5. Output Spectra of CO EDL (Device No. 1). (U)

volume, due to the lower effect of scattering of the primary E-beam, at higher pressures and higher sustainer fields. With the latter, higher electrical pumping rates will be possible, allowing more meaningful parametric investigation of line selection and energy extraction efficiency at lower vibrational bands. This is planned for the next period of this program.

6.0 THE NOMINAL 10-LITER LASER SYSTEM - by M. Mann

(U) During this reporting period, construction of the nominal 10-liter device and integration of associated apparatus and instrumentation were completed and testing was initiated. This device is conceptually similar to the nominal one liter device described previously. However, the gas conditioning and flow system have been refined to insure that the criteria for diffraction limited performance can be satisfied. The various elements of this second laser system are described in the sections below followed by a review of initial experimental results and problems which have limited initial performance to output energies of only 100 to 200 J/pulse.

6.1 The Laser Plenum. (U) Figure 6.1 shows a schematic cross section of the plenum design. Final temperature conditioning of the laser gas is accomplished in a multi-tube liquid nitrogen cooled trimming heat exchanger which is integral with the anode structure. After leaving the trimming heat exchanger the gas flows through a distribution channel on the top of the anode and through a series of screens to insure uniformity of the delivered gas. The gas then flows across the discharge channel transverse to the optical axis, through the cathode structure, and is extracted through a pair of manifolds between the cathode and gun. The extracted gas provides a thermal buffer between the liquid nitrogen reservoir and the ambient conditions external to the plenum. The liquid nitrogen side walls are employed to eliminate the possibility of arcs along the side walls resulting from warm boundary layers. The major elements of the structure are fabricated from hot-formed lexan.

6.2 Flow Control and Gas Conditioning. (U) The flow control and gas conditioning system is designed to provide a mass flow of 5 - 50 grams

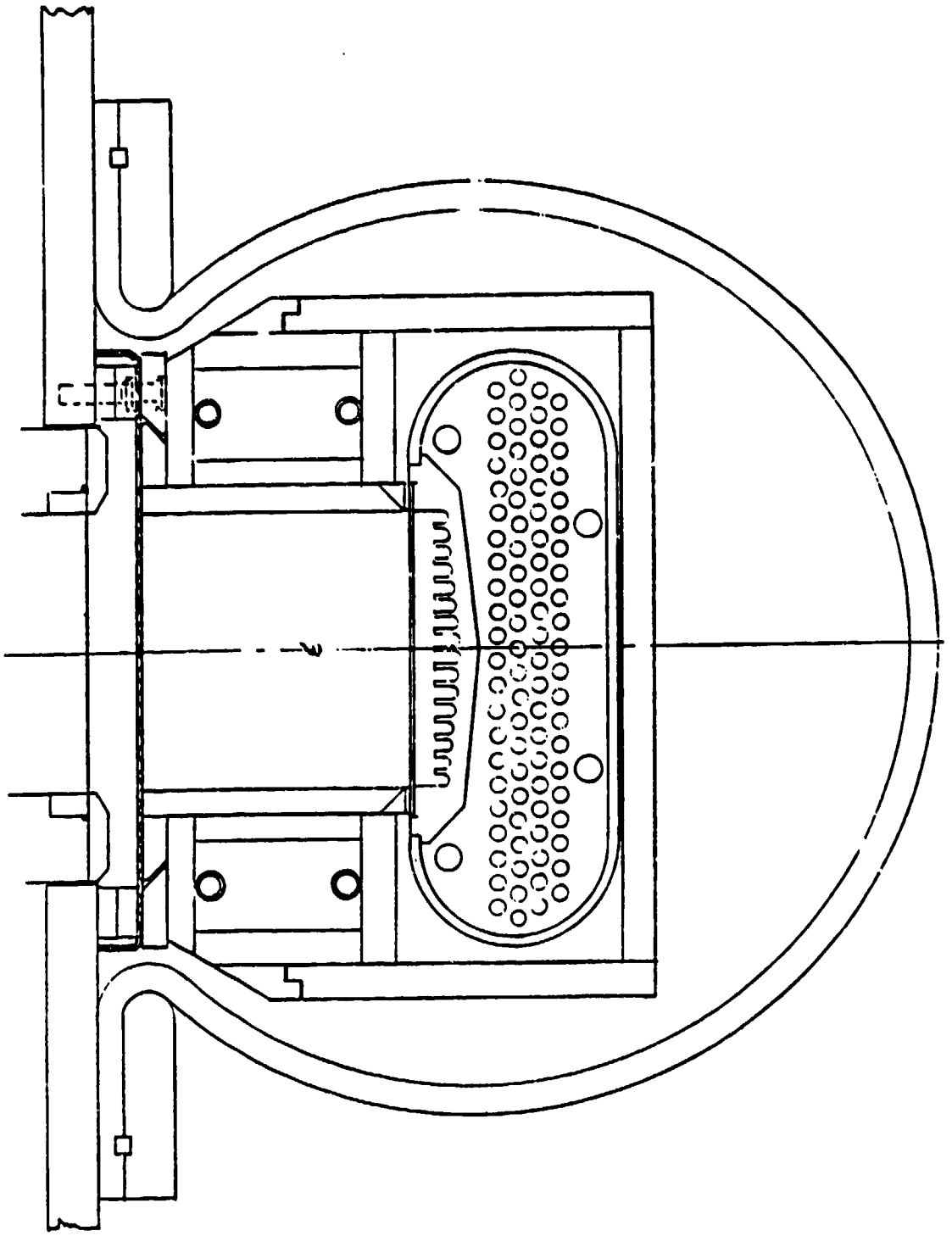

(U) Figure 6.1. Cross Section of 10 Liter Device. (U)

per second which is sufficient for the planned single pulse experiments. The required flow control for the primary constituent gases (CO, N_2, Ar and He) is provided by a system of double stage dome regulators and choked orifices. The individual gases are mixed in a vortex mixing chamber before entering the primary heat exchanger. The pressure in the discharge is maintained at preset values between 50 and 760 torr, independent of flow rate, by a vacuum regulator interposed between the extraction manifold and pump.

(U) The design of the heat exchanger is indicated schematically in Figure 6.2. It was designed to provide temperature conditioned gas which is uniform to less than $\pm 0.5^{\circ}C$. Both the roughing and trimming heat exchangers are included in a single envelope. In order to satisfy the critical temperature requirements, it is necessary to provide circulation of the liquid nitrogen coolant inside the heat exchanger. This is accomplished using a principle very similar to the common aquarium pump. Bubble formation in the roughing section of the heat exchanger lowers the liquid density thus causing an imbalance in hydrostatic pressure. The resultant LN_2 velocity which stirs the coolant is approximately 1.4 m/s. A liquid nitrogen cooled gas transfer tube is employed between the heat exchanger and laser to prevent any degradation in the gas uniformity during transport. Measurements of the temperature uniformity and temporal stability of the gas exiting the heat exchanger show that the objective of $\pm 0.05^{\circ}C$ has been realized.

(U) When high partial pressures of either CO or Ar are used, it is necessary that the gas temperature be greater than $77^{\circ}K$ to avoid liquefication. The required temperature adjustment is made by controlling the back pressure on the liquid nitrogen reservoirs in the heat exchanger, anode, and side walls.

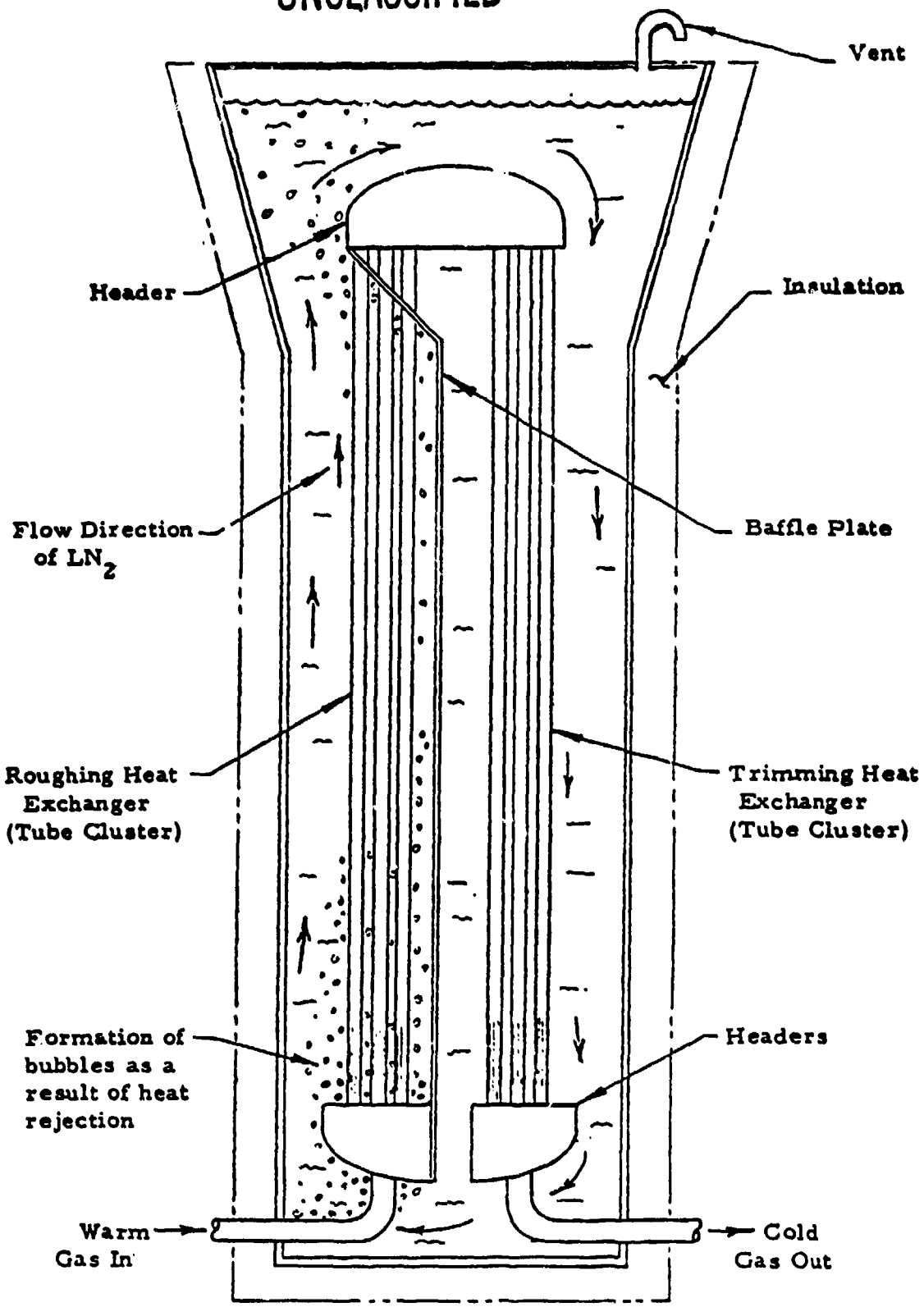

(U) Figure 6.2. Self-stirring cryogenic boiler heat exchanger. (U)

6.3 Optics and Line Selection Cell. (U) Evacuated cells between the laser plenum and the mirrors, described in a previous report, are employed to eliminate heat leaks at the ends of the discharge section. Three inch diameter calcium fluoride windows are currently being used for the initial experiments. However to make use of the optimum volume, four inch round or square optics will be employed as soon as satisfactory cryogenic mounts are completed.

(U) Stable resonators with hole coupled output mirrors are being employed for the initial laser experiments. This will be replaced with a simple unstable resonator and finally a compound resonator for beam quality and line selection experiments. Most of the components for the latter resonator configurations have been completed. The compound unstable resonator is shown schematically in Figure 6.3. The inner resonator beam is expanded in the region of the line selection cell to reduce the optical loading and consequent acoustical disturbances to an acceptable level. The area ratio in the initial resonator will be approximately 100:1.

(U) The required line selection cell and temperature control oven have been completed. The cell has a length of 75 cm and a clear aperture diameter of 14 cm. The oven provides uniform temperatures from ambient to 200°C. The cell can be operated over a pressure range from ~0.01 torr to 5 atm of water vapor and additive broadening gases. This line selection cell will be tested shortly with the one liter device and will be incorporated with the 10-liter device in about a month.

6.4 The Electron Gun. (U) The 10 cm x 100 cm filamentary cathode electron gun has been completed and successfully tested. Nominal operating conditions are an accelerating voltage of 200 kV and a gun current of

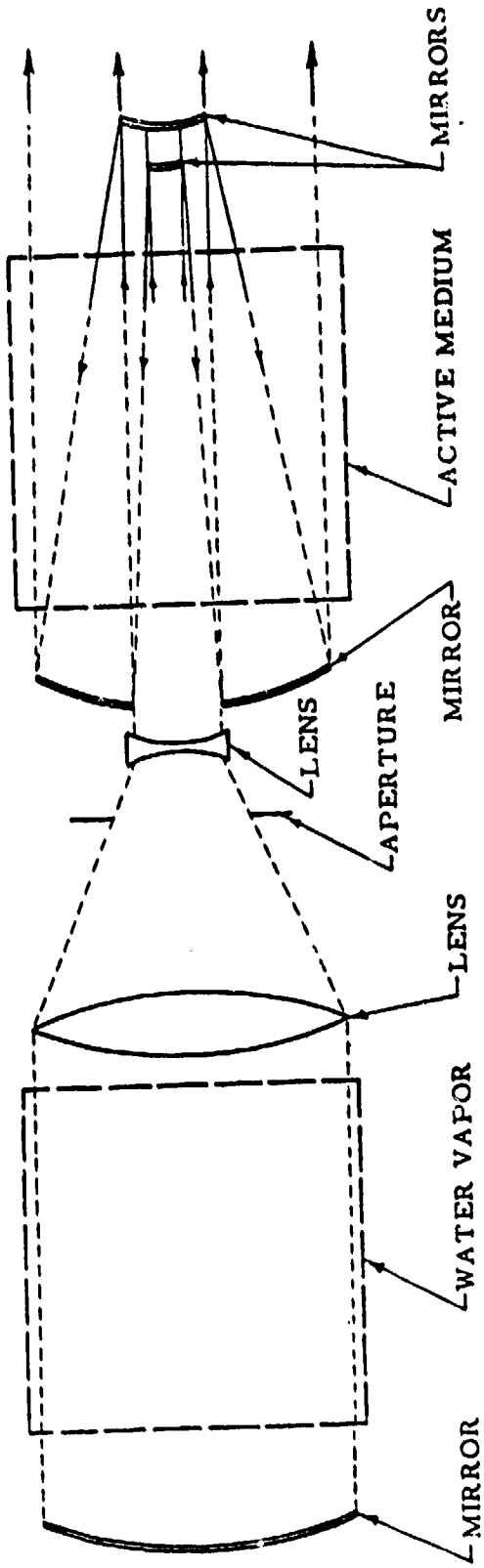

(U) Figure 6.3. Optical configuration for line selected laser. (U)

100 - 140A. Maximum test conditions have been 250 kV and 240A. The beam transmission through the foil and support assembly and sustainer cathode is approximately 50%, in close agreement with expectation. During early testing, difficulty was encountered with oscillations when the gun was operated at high beam current densities under space charge conditions. This problem was controlled by introducing negative feedback between the cathode and grid circuits.

(U) The gun is of a metal-ceramic construction and employs metal seals. It has an operating base pressure of 2×10^{-8} torr. An SF_6 filled shroud encloses the high voltage feedthrough assembly so that there are no high voltage terminals exposed. A shutter assembly is included in the vacuum chamber behind the foil. This permits rapid high voltage aging of the gun by eliminating the possibility of foil punctures due to vacuum arcing.

6.5 Experimental Configuration. (U) The experimental configuration is indicated in the photograph of Figure 6.4. The electron gun and laser chamber are supported from an I-beam frame while the optics are independently mounted on an aluminum box optical rail suspended on air mounts for vibration isolation. The necessary relative motion between the two assemblies is provided by the bellows as seen in the photograph. The initial diagnostic instrumentation is similar to that used in the one liter device, previously described.

6.6 Experimental Results. (U) The initial experiments have been directed at demonstrating the proper functioning of all the elements of the experimental system. Initial temperature measurements of the laser medium showed no transverse gradients but did indicate an axial variation of approximately 2°.

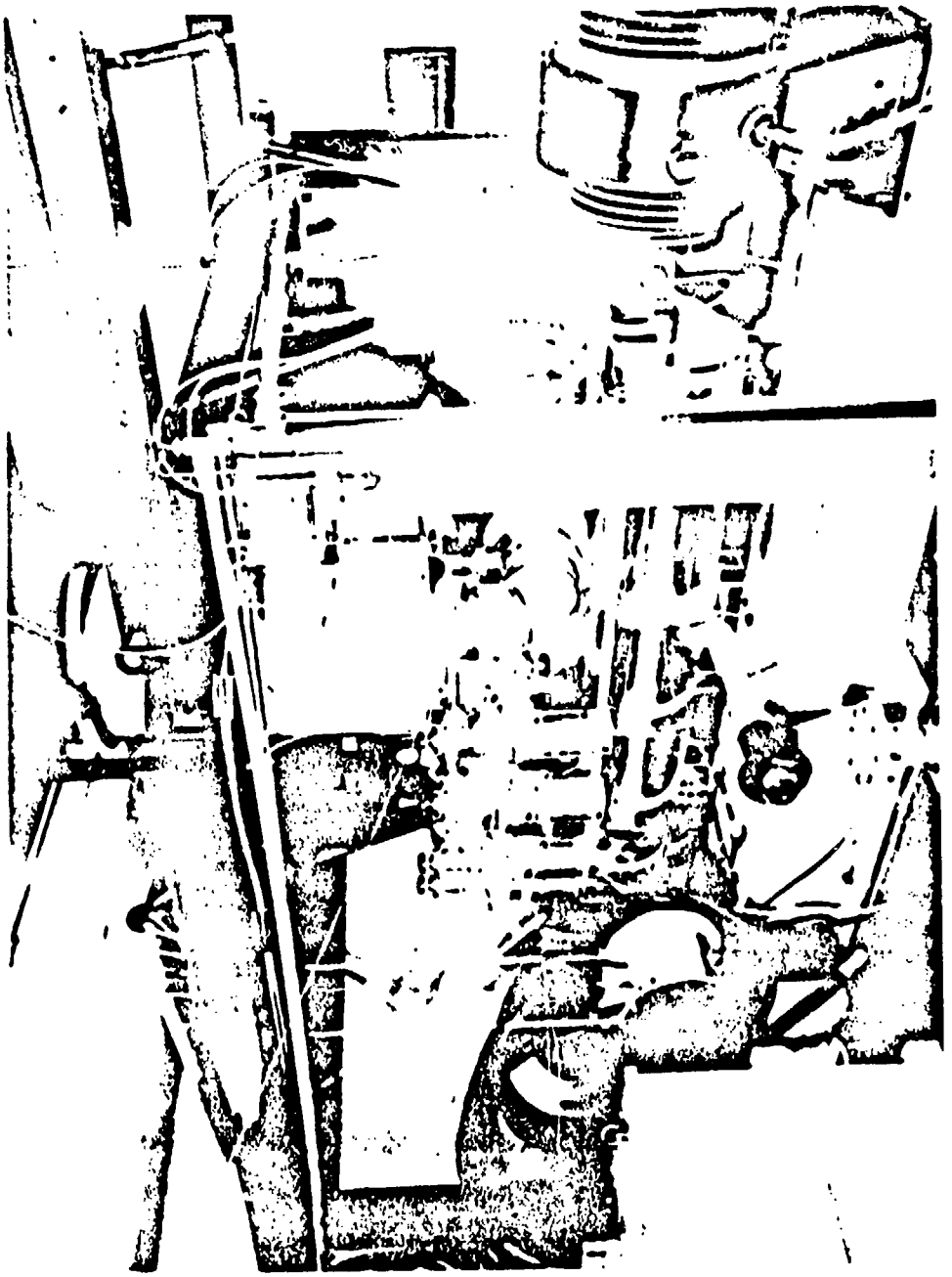

(U) Figure 6.4. Experimental configuration of the 10-liter device. (U)

It was determined that the axial gradient arose from incomplete filling of the anode heat exchanger and this problem has since been remedied. Initial interferometric measurements of the medium, using the helium neon laser in a Michelson interferometer, showed the medium to be stable to within $\lambda/2$ at the helium wavelength at the operating temperature and at all pressures up to 760 torr. Additional interferometric investigations will be performed during the coming period. Measurement of the side wall temperature showed the side walls to be at or below the medium temperature.

(U) For the initial laser experiments, the optical volume was restricted to approximately 3 liters. Typical output energies of 165 J/pulse have been obtained in 1:2:3 $CO:N_2:Ar$ mixtures at approximately 150 torr and 80°K. The sustainer voltage was 12 kV, the sustainer current approximately 1600 A, and the pulse duration was approximately 70 μs. These results are consistent with the results from the one liter device under similar excitation conditions. Performance of the device has been limited to low E/N values ($\sim 10^{-16}$ V cm^2) due to arcing problems at higher sustainer voltages. However the initial experiments did indicate that the device was operating as expected and that once the arcing problems are remedied the objective performance should be realized.

(U) Two specific areas where arcs occur have been isolated and remedies are being implemented. The first problem area is the cold windows which are located between the sustainer electrodes. The high dielectric constant of the window materials leads to field concentration in localized regions of the window mount assembly which has caused punch through on several occasions. Secondly, pin-hole leaks in the window seal permit the discharge to propagate along a preferred path through the seal and along the back side of the window where the pressure is reduced. The resultant arcs have caused fracture of several calcium fluoride windows. This problem has been controlled by improving the window seals and modifying

the mount structures. An alternate configuration in which an impacting jet aerodynamic window is employed to remove the window from the high field region is also being developed.

(U) Another problem which has been encountered is arcing along and behind the discharge sidewalls. The problem again appears to result from field concentrations in the small gaps between the dielectric side walls and the cathode surface. This problem will be eliminated by a slight change in geometry or the addition of a field shaping electrode.

(U) With the existing configuration, measurements indicate standoff voltages of over 25 kV. This is sufficient for the experiments planned for the coming period. These will include beam quality and line selection measurements at 500 J/pulse laser output conditions.

7.0 REFERENCES (U)

1. Northrop Report, NRTC 73-43R, Scaling Generalizations for a Pulsed CO EDL, W. B. Lacina, October 1973.

2. Northrop Report, NRTC 72-10R, High Power CO Laser, Fourth Quarterly Technical Report, September 1972 (Secret).

3. Northrop Report, NRTC 73-10R, High Power CO Laser, Semi-annual and Fifth Quarterly Technical Report, March 1973 (Secret).

4. Northrop Report, NRTC 73-33R, Improved Mode Properties of Unstable Resonators with Tapered Reflectivity Mirrors and Shaped Apertures, G. McAllister, W. Steier, and W. Lacina, August 1973.

5. Yu. A. Anan'ev, "Unstable Resonators and Their Applications (Review)," Sov. J. Quant. Elect. 1, 565. May/June 1972.

6. M. Born and E. Wolfe, Principles of Optics, The MacMillian Company, New York, New York, 1964.

7. A. E. Siegman and R. W. Arrathoon, "Modes in Unstable Optical Resonators and Lens Waveguides," IEEE J. Quant. Elect. QE-3, 156, April 1967.

8. R. M. Osgood, Jr., W. C. Eppers, Jr., and E. R. Nichols, "An Investigation of the High Power CO Laser," IEEE J. Quant. Elect., QE-6, No. 3, pp 145-154, March 1970.

9. N. Legay-Sommaire and F. Legay, "Vibration Distribution of Populations and Kinetics of the CO-N_2 System in the Fundamental and Harmonic Regions," Can. J. Phys., [illegible], pp 1966-1983, September 1970.

10. M. L. Bhaumik, "High Efficiency CO Laser at Room Temperature," Appl. Phys. Letters, 17, No. 5, p 188, 1970.

11. W. B. Lacina, M. M. Mann, R. G. Eguchi, and M. L. Bhaumik, "Efficiency Enhancement and Room Temperature Operation of the CO Laser," Sixth Intern. Conf. on Quantum Electronics, Kyoto, 1970, Digest of Technical Papers, p 374.

12. N. N. Sobolev and V. V. Sokovikov, "The Carbon Monoxide Laser. A Review of Experimental Results," Sov. J. Quant. Electron. Vol. 2, No. 4, pp 305-317, January/February 1973.

[redacted]

DEPARTMENT OF THE NAVY
OFFICE OF NAVAL RESEARCH
800 NORTH QUINCY STREET
ARLINGTON, VA 22217-5660

IN REPLY REFER TO

5510/6
Ser 93/891
8 Oct 98

From: Chief of Naval Research
To: Administrator
Defense Technical Information Center
ATTN: William Bush, DTIC-OCQ
8725 John J. Kingman Road Suite 0944
Ft. Belvoir, VA 22060-6218

Subj: CHANGE OF DISTRIBUTION STATEMENT

1. Permission is granted to change the distribution statement for the following documents to Distribution Statement A: Approved for Public Release; Distribution is Unlimited:

AD 527 922
AD 523 538

2. Questions may be directed to the undersigned on (703) 696-4619.

PEGGY LAMBERT
By direction